PCCP

PAPER

View Article Online
View Journal | View Issue



Cite this: *Phys. Chem. Chem. Phys.*, 2016, **18**, 3730

# Structure and dynamics of the aliphatic cholesterol side chain in membranes as studied by $^2$H NMR spectroscopy and molecular dynamics simulation†

Alexander Vogel,[a] Holger A. Scheidt,[a] Dong Jae Baek,[bc] Robert Bittman‡[c] and Daniel Huster*[a]

Cholesterol is an evolutionarily highly optimized molecule particularly known for its ability to condense the phospholipids in cellular membranes. Until recently, the accompanying increase in the chain order of the surrounding phospholipids was attributed to the planar and rigid tetracyclic ring structure of cholesterol. However, detailed investigations of cholesterol's aliphatic side chain demonstrated that this side chain is responsible for approximately half of the condensation effect. Therefore, we investigated the structure and dynamics of the aliphatic side chain of cholesterol using $^2$H solid-state nuclear magnetic resonance (NMR) spectroscopy and microsecond timescale all-atom molecular dynamics (MD) simulations in four different model membranes: POPC, DPPC, PSM, and POPC/PSM (1 : 1 mol/mol) and at three different temperatures: 5 °C, 37 °C, and 50 °C. A cholesterol variant, in which 11 hydrogens of the aliphatic side chain were exchanged for deuterium, was used and the respective $^2$H NMR spectra confirmed the axially asymmetric rotational diffusion of cholesterol in DPPC and PSM. Furthermore, NMR spectra indicated that some hydrogens showed an unexpected magnetic inequivalency. This finding was confirmed by all-atom molecular dynamics simulations and detailed analysis revealed that the hydrogens of the methylene groups at C22, C23, and C24 are magnetically inequivalent. This inequivalency is caused by steric clashes of the aliphatic side chain with the ring structure of cholesterol as well as the branched C21 methyl group. These excluded volume effects result in reduced conformational flexibility of the aliphatic side chain of cholesterol and explain its high order (order parameter of 0.78 for chain motions) and large contribution to the condensation effect. Additionally, the motional pattern of the side chain becomes highly anisotropic such that it shows larger fluctuations perpendicular to the ring plane of cholesterol with a biaxiality of the distribution of 0.046. Overall, our results shed light on the mechanism how the aliphatic side chain is able to contribute about half of the condensation effect of cholesterol.

Received 26th August 2015,
Accepted 6th January 2016

DOI: 10.1039/c5cp05084g

www.rsc.org/pccp



## Introduction

Cholesterol is one of the most abundant bulk lipids in cellular membranes and plays the key role in the phase behavior and lateral organization of the plasma membrane.[1] Specific interactions between cholesterol and sphingolipids are believed to represent the driving force for the domain structure of membranes consisting of cholesterol-depleted liquid-disordered ($l_d$) and cholesterol-enriched liquid-ordered ($l_o$) domains.[2–4] However, as of now, there is no complete understanding of what brings about the complicated dynamic domain structure of the plasma membrane and of the role cholesterol plays in these dynamic domain forming processes.[5–8]

Cholesterol preferentially interacts with saturated lipid chains.[9–11] Attractive van der Waals interactions between the smooth α-face of cholesterol's planar and rigid ring structure and the lipid chains have been assumed to be responsible for this effect,[12,13] which leads to a drastic increase in the lipid packing density that is called condensation.[14] However, a recent report demonstrated that the iso-branched aliphatic side chain of cholesterol also plays an important role in the interaction with phospholipid chains and surprisingly accounts for 40–60% of

[a] *Institute of Medical Physics and Biophysics, University of Leipzig, Härtelstr. 16-18, 04275 Leipzig, Germany. E-mail: daniel.huster@medizin.uni-leipzig.de; Fax: +49 (0)341 97 15709; Tel: +49 (0)341 97 15701*
[b] *College of Pharmacy and Natural Medicine Research Institute, Mokpo National University, Jeonnam, Republic of Korea*
[c] *Department of Chemistry and Biochemistry, Queens College of the City University of New York, Flushing, NY 11367-1597, USA*

† Electronic supplementary information (ESI) available. See DOI: 10.1039/c5cp05084g

‡ Prof. Dr Robert Bittman passed away on 1 October 2014.

the condensation effect.[15] This result was also confirmed by recent molecular dynamics (MD) simulations.[16] Sterols bearing an unbranched side chain also promote lipid condensation, but to a lesser extent than the native branched iso-alkyl chain of cholesterol.[17]

There is relatively little published work on the structural and dynamical aspects of the aliphatic side chain of cholesterol as opposed to the large body of literature on the order and dynamics of phospholipid chains.[18–20] In particular, quadrupolar $^{2}H$ and dipolar $^{1}H$–$^{13}C$ NMR order parameters have advanced our understanding of the influence of cholesterol on lipid packing, lateral organization, and domain formation in model membrane systems.[11,21–23] In a first investigation of the cholesterol side chain, it was found that the two chemically identical methyl groups C26 and C27 (see Fig. 1 for the Nomenclature) did not provide equivalent $^{2}H$ NMR signals.[24] This was further confirmed by Dufourc *et al.* for the C24 methylene group.[25] For the methylene segments of the cholesterol side chain, much higher order parameters were found compared to phospholipid acyl chains, also the aforementioned inequivalence between the two protons of the same methylene group has only been observed in phospholipid chains for the C2 segments. As a consequence of a very elaborated analysis of these experimental findings, the cholesterol side chain was pronounced to be "as ordered as the condensed ring structure".[25] However, the very low quadrupolar splittings of the terminal methyl groups of C26 and C27, observed in $^{2}H$ NMR spectra, have not been understood in the framework of this model.[25]

In addition to $^{2}H$ NMR studies, $^{13}C$ NMR separated local field experiments under magic-angle spinning conditions have proven very useful to study the order parameters of molecular segments of biomolecules[26,27] and in particular lipids and cholesterol.[23,28–30] In a recent paper, the order parameters of cholesterol were also determined by this method, though at lower resolution than in the $^{2}H$ NMR studies.[28] Experimental results were also compared to a 100 ns MD simulation. The simulated $^{1}H$–$^{13}C$ order parameters showed good agreement with the previously published $^{2}H$ NMR data. Also, simulation and experiment showed reasonable agreement for the ring structure of cholesterol but not for the side chain, where the MD results were too small by a factor of $\sim$2, possibly due to the united atom GROMOS force field[31] or the short simulation time.

Clearly, a better understanding of the putatively rigid cholesterol side chain with the highly mobile phospholipid chains will advance our understanding of the lateral organization of the lipid molecules in the membrane and their relevance for the organization of biological membranes. Here, we focus on the structural and dynamical behaviour of the aliphatic cholesterol side chain by analyzing the $^{2}H$ NMR spectra of a chain deuterated cholesterol-$d_{11}$ molecule[32] in POPC, DPPC, PSM, as well as in a model lipid raft mixture and four all-atom MD simulations, each of more than 1.5 μs length.

Using these methods we could show that some conformations of the side chain result in steric clashes with the ring structure of cholesterol and therefore are forbidden. This can be interpreted as a reduction of the volume that is accessible to the side chain and leads to high chain order and anisotropic chain motions.

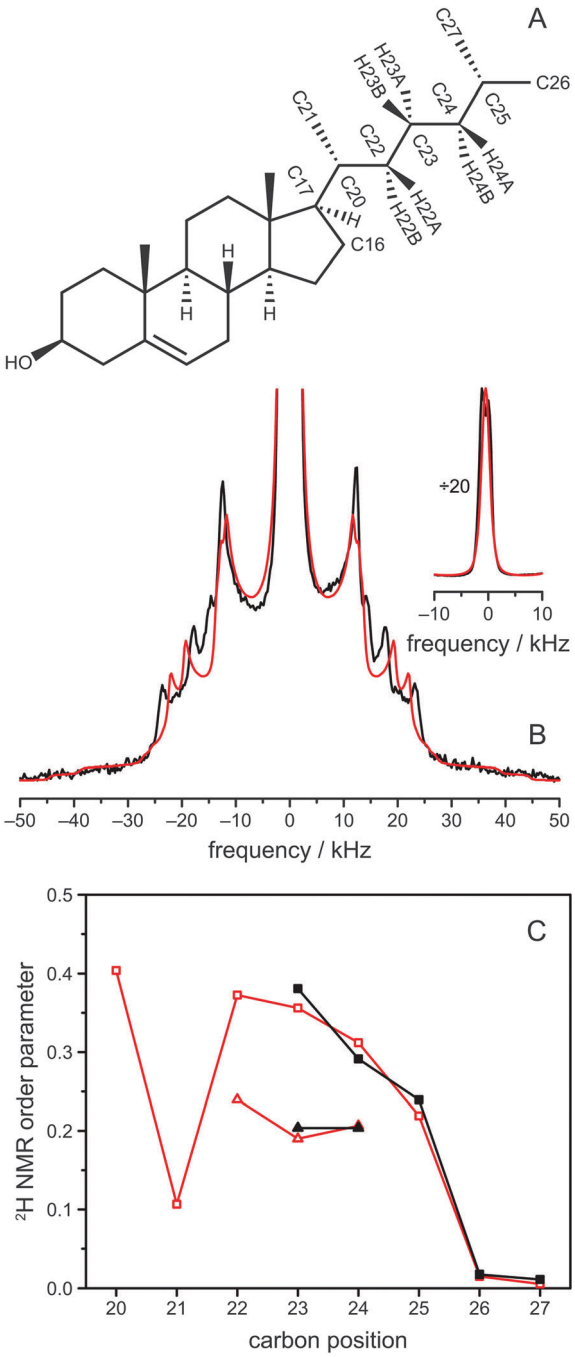


Fig. 1 (A) Chemical structure of cholesterol including the relevant nomenclature. In cholesterol-$d_{11}$, hydrogens were replaced by deuterium at positions C23, C24, C25, C26, and C27. (B) $^{2}H$ NMR spectra of POPC/cholesterol-$d_{11}$ (3 : 1 mol/mol) at 37 °C. The experimentally obtained $^{2}H$ NMR spectrum is shown in black, while the spectrum calculated from the MD simulation is drawn in red. The inset shows the same spectrum vertically divided by a factor of 20 to show the intense Pake doublets from the two terminal $CH_3$ groups. (C) Corresponding $^{2}H$ NMR order parameters of the aliphatic cholesterol side chain. Experimental data is shown in black for all deuterated carbon positions of cholesterol-$d_{11}$, while the order parameters from MD simulation, which are shown in red, were calculated for the whole chain. Data for C22, C23, and C24 shows two values because A (triangles) and B (squares) hydrogens are not magnetically equivalent at these positions. In the MD simulation data, the three hydrogens of the $CH_3$ groups at C21, C26, and C27 are averaged, because their order parameters differ by less than 0.002. The first 500 ns were considered as equilibration of the MD simulation and omitted for data evaluation.

# Materials and methods

## Materials

The lipids 1-palmitoyl-2-oleoyl-*sn-glycero*-3-phosphocholine (POPC), 1,2-dipalmitoyl-*sn-glycero*-3-phosphocholine (DPPC) and *N*-palmitoyl-D-*erythro*-sphingosylphosphorylcholine (PSM) were purchased from Avanti Polar Lipids, Inc. (Alabaster, Al) and used without further purification. Cholesterol-$d_{11}$ was synthesized as described in literature.[32]

## Sample preparation

For the $^2$H NMR measurements, cholesterol-$d_{11}$ was mixed with the individual phospholipids in chloroform at a molar ratio of 1 : 3 (25 mol% cholesterol-$d_{11}$). In addition, a lipid raft mixture of POPC/PSM/cholesterol-$d_{11}$ at a molar ratio of 37.5/37.5/25 mol/mol/mol was prepared. After the removal of the chloroform using a vacuum evaporator, the samples were redissolved in cyclohexane and lyophilized. Samples were hydrated with 40 wt% deuterium-depleted $H_2O$ and equilibrated by ten freeze-thaw cycles and gentle centrifugation.

## $^2$H NMR spectroscopy

The static $^2$H NMR spectra were recorded on a Bruker Avance I 750 MHz NMR spectrometer (Bruker Biospin GmbH, Rheinstetten, Germany) at a resonance frequency of 115.1 MHz for $^2$H using a single-channel probe with a 5 mm coil. The spectra were acquired with a phase-cycled quadrupolar echo sequence.[33] The typical length of the 90° pulses was around 3 μs, the relaxation delay was 1 s.

## Molecular dynamics simulations

Four all-atom MD simulations were carried out: two simulations of a POPC/cholesterol at 37 °C and 50 °C, one simulation of DPPC/cholesterol at 50 °C, and one simulation of PSM/cholesterol at 50 °C. The most detailed data analysis was conducted on the POPC/cholesterol simulation at 37 °C. Each simulation consisted of 150 phospholipids (POPC, DPPC, PSM), 50 cholesterols, and TIP3 water and was run for ~1550 ns. Setup of the membranes was conducted according to published procedures.[34] Particular attention was paid to avoid any molecule from being threaded through one of the cholesterol rings. The program NAMD[35] was employed for the simulation under conditions of normal pressure (1.013 bar), using the most recent CHARMM all-H C36 lipid force field[36] and the modified C36c force field[37] for cholesterol. This allowed to run the simulation with flexible surface area and therefore enabled the system to adapt to the condensation effect of cholesterol (no additional force was applied in the plane of the membrane). The PSM force field values were taken from literature.[38] The smooth particle mesh Ewald algorithm was used to compute the electrostatic forces[39] and the SHAKE algorithm was used to keep rigid all bonds involving hydrogen atoms, allowing a 2 fs time step.[40]

# Results

$^2$H solid-state NMR spectroscopy represents a very suitable tool to obtain detailed information on the structure and dynamics of the aliphatic side chain of cholesterol.[24,25] In such spectra, a Pake doublet is observed for each deuterium in the molecule, where the magnitude of the splitting of the doublet is determined by the possible orientations of the C–$^2$H bond with respect to the membrane normal and directly proportional to the motional amplitude of this bond.[41,42] Sophisticated models have been developed to interpret these quadrupolar splittings in terms of orientation and dynamics of the deuterated molecule.[25,43–45]

Here, we have used a specifically deuterated cholesterol-$d_{11}$, in which the hydrogen atoms attached to C23, C24, C25, C26 and C27 were replaced by deuterium, acting as probes in our samples (Fig. 1A).[32] This cholesterol variant was mixed with various phospholipids to investigate the influence of the lipid environment on the aliphatic cholesterol side chain. The $^2$H NMR spectrum of the sample of POPC/cholesterol-$d_{11}$ (molar ratio 75 : 25) at 37 °C is shown in black in Fig. 1B and consists of a superposition of several Pake doublets. There is a very intense Pake doublet with very small quadrupolar splitting, which can be assigned to the deuterons of the methyl groups at C26 and C27 due to the fast rotation of the $CH_3$ groups in agreement with literature.[25] In addition to this spectral component, four more Pake patterns with larger quadrupolar splittings are clearly visible, which originate from the five deuterons at C23, C24, and C25. As shown before, the two deuterons of the C24 segment of cholesterol are not equivalent.[25] Therefore, to obtain a total of four Pake patterns, we expected the two deuterium atoms on C23 to be equivalent and give rise to one Pake doublet with double intensity. This doublet should have the largest quadrupolar splitting (*i.e.*, highest order) because it was shown that the deuterons on C22 are equivalent and of higher order than on C24,[25] and we expected C23 to be of intermediate order. In our NMR spectrum, however, the innermost Pake doublet (aside from the $CH_3$ doublets) showed double intensity.

Since it is not straightforward to assign the individual Pake doublets to the carbon positions in the aliphatic cholesterol side chain, we conducted an all-atom MD simulation of the same system. The simulation consisted of 150 POPC and 50 cholesterol molecules, which were simulated for ~1.5 μs at 37 °C. From the simulation, the angles $\beta$ of all C–H bonds in the aliphatic cholesterol side chain with respect to the membrane normal were extracted and subsequently converted into order parameters $S_{CD}$ *via*

$$S_{CD} = 1/2(3\cos^2\beta - 1).^{45}$$

These order parameters were used to assign our experimental spectrum. A direct comparison between order parameters from experiment and MD simulation is shown in Fig. 1C and the respective numbers are provided in Table 1. Overall, excellent agreement is observed and the average order parameter of the MD simulation is only 4.3% smaller than that of the experiment in contrast to previous MD simulations, where the order parameters differed by a factor of ~2.[28] With these parameters in hand, the $^2$H NMR spectrum expected from the MD simulation can be calculated and compared to the experimental data. In Fig. 1B the simulated $^2$H NMR spectrum is superimposed by the experimental spectrum; once again, very good agreement

Table 1 Order parameters determined for the aliphatic cholesterol chain in POPC/cholesterol (3 : 1 mol/mol) at several temperatures from experimental $^2$H NMR spectra and MD simulations. The first 500 ns were considered as equilibration of the MD simulation and omitted for data evaluation

| | 5 °C | 37 °C | | 50 °C | |
|---|---|---|---|---|---|
| | NMR | NMR | MD | NMR | MD |
| H20 | n.d.[a] | n.d. | 0.4040 | n.d. | 0.3954 |
| H21A | n.d. | n.d. | 0.1058 | n.d. | 0.1035 |
| H21B | n.d. | n.d. | 0.1070 | n.d. | 0.1026 |
| H21C | n.d. | n.d. | 0.1072 | n.d. | 0.1035 |
| H22A | n.d. | n.d. | 0.2396 | n.d. | 0.2232 |
| H22B | n.d. | n.d. | 0.3726 | n.d. | 0.3591 |
| H23A | 0.2771 | 0.2036 | 0.1900 | 0.1804 | 0.1719 |
| H23B | 0.4256 | 0.3808 | 0.3562 | 0.3617 | 0.3402 |
| H24A | 0.2771 | 0.2036 | 0.2065 | 0.1804 | 0.1877 |
| H24B | 0.3497 | 0.2914 | 0.3120 | 0.2715 | 0.2938 |
| H25 | 0.3114 | 0.2395 | 0.2190 | 0.2140 | 0.1982 |
| H26A | | | 0.0155 | | 0.0136 |
| H26B | 0.0224 | 0.0176 | 0.0154 | 0.0176 | 0.0142 |
| H26C | | | 0.0144 | | 0.0148 |
| H27A | | | 0.0056 | | 0.0053 |
| H27B | 0.0176 | 0.0112 | 0.0050 | 0.0096 | 0.0047 |
| H27C | | | 0.0059 | | 0.0050 |

[a] Not determined due to the lack of deuteration.

between experiment and simulation is observed. This means that the MD simulation of 1.5 μs length was able to fully sample the orientation and dynamics of the aliphatic side chain of cholesterol with high accuracy and can be used to further analyze the details of the system.

The observed $^2$H NMR quadrupolar splitting $\Delta\nu_Q$ is directly related to the angle $\beta$ between the C–$^2$H bond and the membrane normal *via*

$$\Delta\nu_Q = 3/4\chi_Q(3\cos^2\beta - 1),$$

where $\chi_Q$ is the static quadrupolar coupling constant that has a value of 167 kHz for aliphatic carbon deuterium bonds.[41,42] As an illustration of the dynamic distribution of the C–D bonds in the cholesterol side chain, histograms of the angle $\beta$ as observed in the MD simulation of POPC/cholesterol are shown in Fig. 2A–C for each individual deuteron on the methyl groups of C22, C23 and C24, respectively (termed A and B, refer to Fig. 1A for their definition). Note that the carbon position C22 was not deuterated in our experiments. Significant differences between the two deuterons are clearly observed. All three B deuterons exhibit a distribution with one distinct maximum, while the A deuterons show a wider distribution with several maxima. This confirms that the deuterons at C22, C23 and C24 are magnetically not equivalent. Data for all other carbon positions of the aliphatic chain is shown in Fig. S1 (ESI†) and the individual deuterons are almost indistinguishable. It is surprising that the deuterons on C22 are not equivalent in our MD simulations because experimental data showed that they exhibit the same quadrupolar splitting.[25]

In the report by Dufourc *et al.*,[25] it has been speculated that the two inequivalent deuterons at C24 have "different average orientations with respect to the axis of segmental motion". However, from the MD simulation we calculated the mean angle $\beta$ for both atoms attached to C24 and found they were

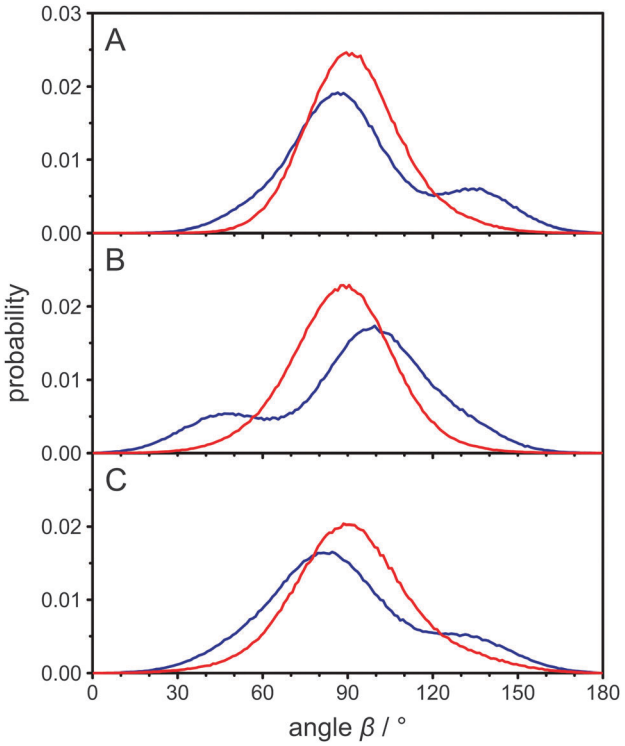


Fig. 2 (A) Histograms of the angle $\beta$ between the two carbon hydrogen bonds attached to C22 and the membrane normal as obtained from the MD simulation of POPC/cholesterol (3 : 1 mol/mol) at 37 °C. Panels (B) and (C) show the same histograms for C23 and C24, respectively. The data for hydrogen A is shown in blue and for hydrogen B in red.

both very similar (89.3° for the A deuteron and 92.2° for the B deuteron). This small alteration is not sufficient to account for the observed differences in the quadrupolar splittings. From the histograms of the angle $\beta$ in Fig. 2C it is clear, however, that the explanation of the inequivalent deuterons in the cholesterol side chain is more complex. Clearly, it is not the average orientation of each bond vector that differs but rather their distribution. To investigate the orientations in some more detail, we also determined the mean rotational axis of cholesterol, which is on average relatively parallel to the membrane normal. Due to the cholesterol wobbling motion, the mean angle between this axis and the membrane normal is 17.1°, while the most probable angle is ~13°. This agrees well with results from other MD simulations.[28,37] We also determined the molecular order parameter of the cholesterol ring system, which is 0.839 in our MD simulation. This value agrees well with experimental results.[25]

Next, we calculated the mean angle between the C24–hydrogen bond and this rotational axis for both hydrogens and again, they were very similar (89.6° for the A hydrogen and 93.0° for the B hydrogen). The histograms of this angle and also for the groups of C22 and C23 are displayed in Fig. S2 (ESI†) and overall show better defined orientations than the histograms in Fig. 2. This is due to the fact that the wobbling motion of cholesterol is not relevant in Fig. S2 (ESI†), as the rotational axis of cholesterol is fixed within the molecule. Nevertheless, the general appearance is

the same and the distributions differ significantly for hydrogens that are bound to the same carbon.

One possible explanation for the observed magnetic inequivalency of the C–H bonds at C22, C23, and C24 are steric clashes within the cholesterol molecule. Therefore, we calculated histograms of the dihedral angles between four consecutive carbons along the aliphatic cholesterol side chain from the MD simulation, which are shown as black lines in Fig. 3. A typical histogram that is expected for four consecutive carbons in a non-branched hydrocarbon chain is observed for the dihedral angle C22–C23–C24–C25 shown in Fig. 3C. The *trans* orientation (dihedral angle $\approx 180^\circ$) is most likely, while the two *gauche* orientations (dihedral angle $\approx \pm 60^\circ$) are less likely, but have identical probability. All other dihedral angles along the chain differ from this expected distribution. For the dihedral angles C17–C20–C22–C23 and C20–C22–C23–C24 the $\approx -60^\circ$ orientation is prohibited. We also extracted these dihedral angles from a total of 38 crystal structures[46–49] and the corresponding histograms are shown as grey bars in Fig. 3. The angles that are forbidden in our MD simulations also did not occur in these crystal structures, while all other possible angles are found at least once in the crystal structures.

To investigate what causes these $-60^\circ$ orientations to be prohibited, we calculated how the cholesterol structure would look like with exactly this orientation at the C17−C20−C22−C23 dihedral angle and all other dihedral angles in the chain in their most likely conformation (Fig. 4A). In this structure, the hydrogens H16B and H23B have a distance of 1.40 Å, which is significantly less than twice the hydrogen van der Waals radius of 1.09 Å.[50] Furthermore, H16A and H23B have a distance of 1.74 Å. Contacts this close are not tolerated and prohibit the dihedral angle to reach $-60^\circ$. The cholesterol structure with the dihedral angle C20–C22–C23–C24 in the $-60^\circ$ orientation is shown in Fig. 4B. In this structure, H21C (since the $CH_3$ group can rotate freely it also could be H21A or H21B) and H24B have a distance of 1.03 Å and therefore display a significant steric clash. For C23–C24–C25–C26 the $\approx -60^\circ$ orientation has a reduced probability while the $+60^\circ$ and $180^\circ$ orientations are virtually equally probable (Fig. 3D). To investigate what causes this distribution, the cholesterol structures with the dihedral angle C23–C24–C25–C26 at $+60^\circ$, $180^\circ$, and $-60^\circ$ are shown in Fig. 4C–E, respectively.

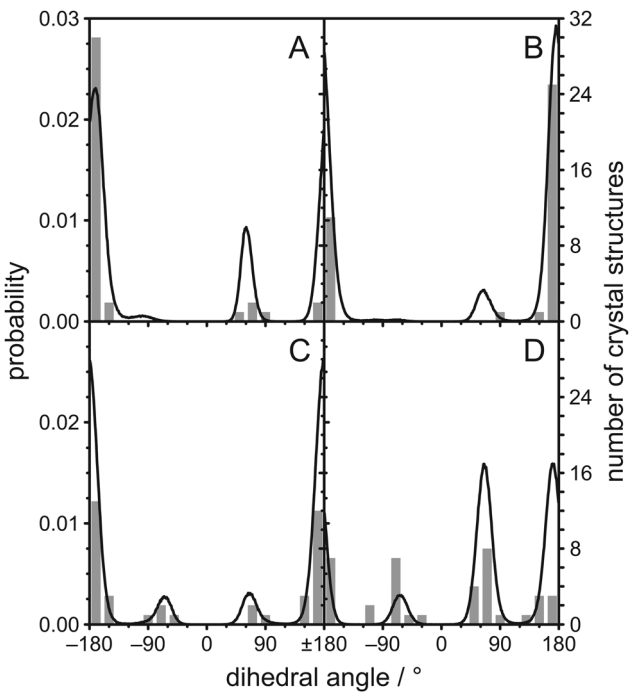


Fig. 3 Histograms of dihedral angles in the aliphatic chain of cholesterol as obtained from the MD simulation of POPC/cholesterol (3 : 1 mol/mol) at 37 °C and from 38 crystal structures found in the literature[46–49] for (A) C17–C20–C22–C23, (B) C20–C22–C23–C24, (C) C22–C23–C24–C25, and (D) C23–C24–C25–C26. Data from the MD simulation is shown as black lines while data from the crystal structures is shown as grey bars.

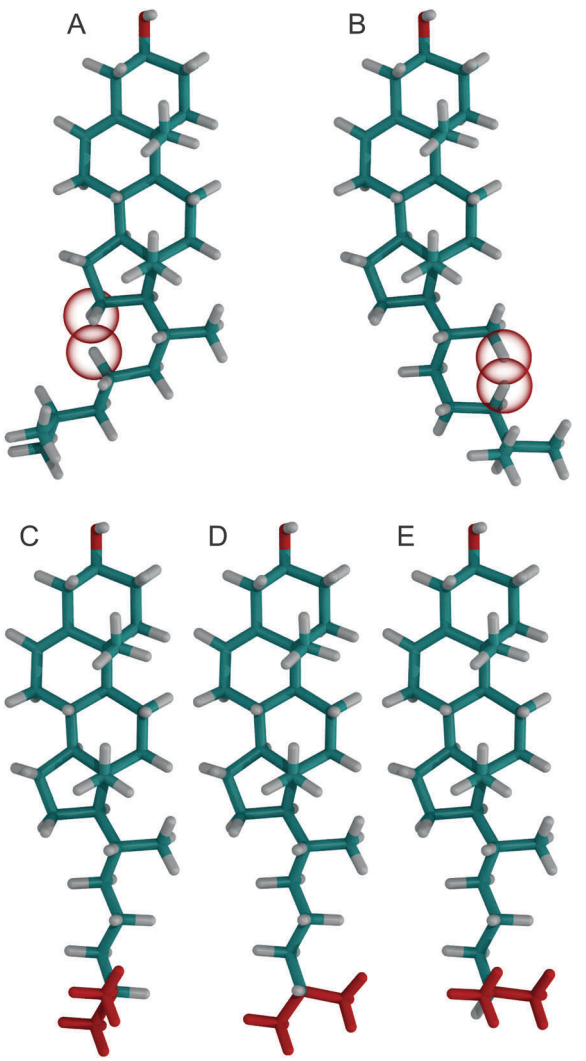


Fig. 4 Cholesterol structures with various dihedral angles, where hydrogens that have the closest steric contact are highlighted by a red sphere with the van der Waals radius of hydrogen. All dihedral angles were in their most likely conformation with the exception of (A) C17–C20–C22–C23 at $-60^\circ$, (B) C20–C22–C23–C24 at $-60^\circ$, (C) C23–C24–C25–C26 at $+60^\circ$, (D) C23–C24–C25–C26 at $180^\circ$, and (E) C23–C24–C25–C26 at $-60^\circ$ respectively. In panels (C)–(E) the two terminal $CH_3$ groups were colored red for better visibility.

In the two similarly likely orientations of +60° and 180°, one of the two $CH_3$ groups is in the *trans* configuration, while in the less likely −60° orientation both $CH_3$ groups are in the *gauche* configuration. Obviously, it is favorable to have at least one of the bulky $CH_3$ groups extended towards the membrane center. However, this distribution might change in an environment with very short lipid chains, where cholesterol might be forced to adapt to the hydrophobic thickness.[51] In the crystal structures however, the +60°, −60°, and 180° orientations have similar probability, which supports our interpretation of a membrane mediated effect that cannot be observed in the crystal structures where no membrane is present.

To investigate how the steric clashes influence the distribution of the angles between the carbon hydrogen bonds and the rotational axis of cholesterol, the cholesterol structures with the dihedral angle C17–C20–C22–C23 in the 180°, +60°, and the prohibited −60° orientation are compared in Fig. 5. In this figure, the A hydrogens at C22, C23, and C24 are colored blue and in the two allowed dihedral angles they have very different orientations with respect to the rotational axis of cholesterol, which is shown in green. This explains why in the histogram (Fig. S2, ESI†) several maxima at different angles are observed. For the B hydrogens, however, in the two allowed dihedral angles the angle between the carbon hydrogen bond and the rotational axis of cholesterol is always close to 90°, explaining the single maximum around 90° in Fig. S2 (ESI†). The dihedral angle of −60° that would cause angles between the carbon hydrogen bond and the rotational axis of cholesterol other than 90° is prohibited by the steric clashes between H16B and H23B as well as H16A and H23B.

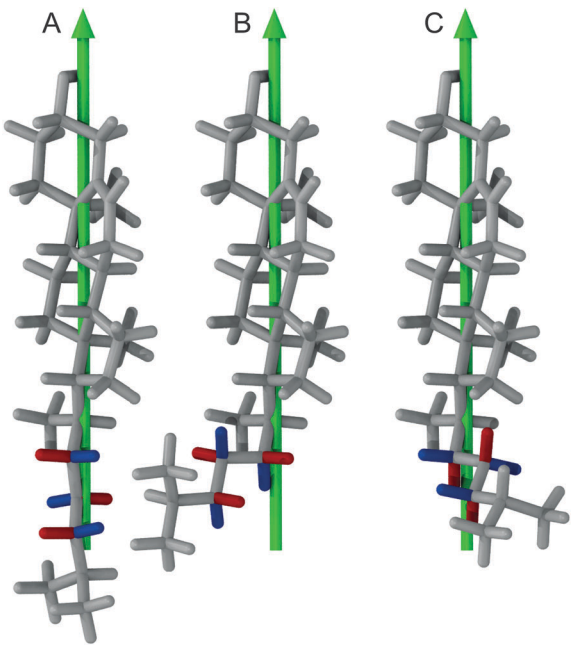


Fig. 5 Cholesterol structures with the dihedral angle C17–C20–C22–C23 in (A) 180°, (B) +60°, and the prohibited (C) −60° orientation respectively. The green arrow indicates the main rotational axis of cholesterol while A hydrogens at C22, C23, and C24 are colored blue and B hydrogens are colored red.

To further investigate the influence of the surrounding phospholipids on the cholesterol molecule and its aliphatic side chain, experiments as well as MD simulations with DPPC, PSM, and a POPC/PSM (1 : 1 mol/mol) mixture (no MD simulation for this system) were conducted. Such binary and ternary systems also represent the essential lipid species in raft mixtures. In Fig. 6, the experimental spectra (black lines) at various temperatures are summarized. All $^2$H NMR spectra with sufficient resolution were fitted (red lines) by a superposition of seven Pake doublets, where quadrupolar splitting, line width, chemical shift, and overall sample ellipticity were adjusted. Good fits were obtained for cholesterol-$d_{11}$ in POPC and POPC/PSM, while fits in DPPC and PSM show clear deviations indicative of slight axially asymmetric motion[25,41,42] even at 50 °C. From these fits, $^2$H NMR order parameters were obtained and assigned in the same sequence as the order parameters derived from the MD simulation of POPC/cholesterol at 37 °C. All order parameters are summarized in Fig. S3 and Table S1 (ESI†) (data for POPC at 37 °C is found in Fig. 1C and Table 1). Comparing the spectral shape and order parameter profile a high similarity is observed between POPC and the POPC/PSM mixture (the average order parameter is higher in the latter) at all temperatures. This indicates that the overall behavior of the aliphatic side chain is similar in both environments on the NMR timescale. In contrast, the $^2$H NMR spectrum of cholesterol-$d_{11}$ in PSM looks quite different, although the order parameters are similar to those in the POPC/PSM mixture. The numerical fits of the spectra clearly show signs of slight axially asymmetric motion, which means that cholesterol might not achieve total rotational symmetry on the NMR timescale of several microseconds even at 50 °C. This indicates that cholesterol rotation is slower in PSM than in POPC/PSM. The same is observed for DPPC.

The order parameters also were extracted from MD simulations of cholesterol in POPC, DPPC, and PSM at 50 °C. Overall, the agreement for the two MD simulations in DPPC and PSM was not as good as for the POPC simulations at 37 °C and 50 °C, but still much better than reported previously.[28] In the POPC MD simulations, the average order parameter was slightly smaller by 4.3% (37 °C) or 3.1% (50 °C) than the experiment. In contrast, it was somewhat bigger by 16.3% and 8.7% in the DPPC and PSM MD simulations, respectively. From the MD order parameters at 50 °C, $^2$H NMR spectra were calculated and a direct comparison to the spectra obtained from experiment is found in Fig. S4 (ESI†) (the comparison for POPC at 37 °C is found in Fig. 1B). Again, differences are small for POPC and larger for DPPC and PSM.

## Discussion

It is well known that cholesterol is an evolutionarily highly optimized molecule. Its most striking effect in membranes is the cholesterol induced condensation of the surrounding phospholipids and the accompanying increase in molecular order and membrane stiffness and a concomitant reduction in membrane permeability.[15,52] No matter which modifications of the cholesterol structure are tested, none of them can

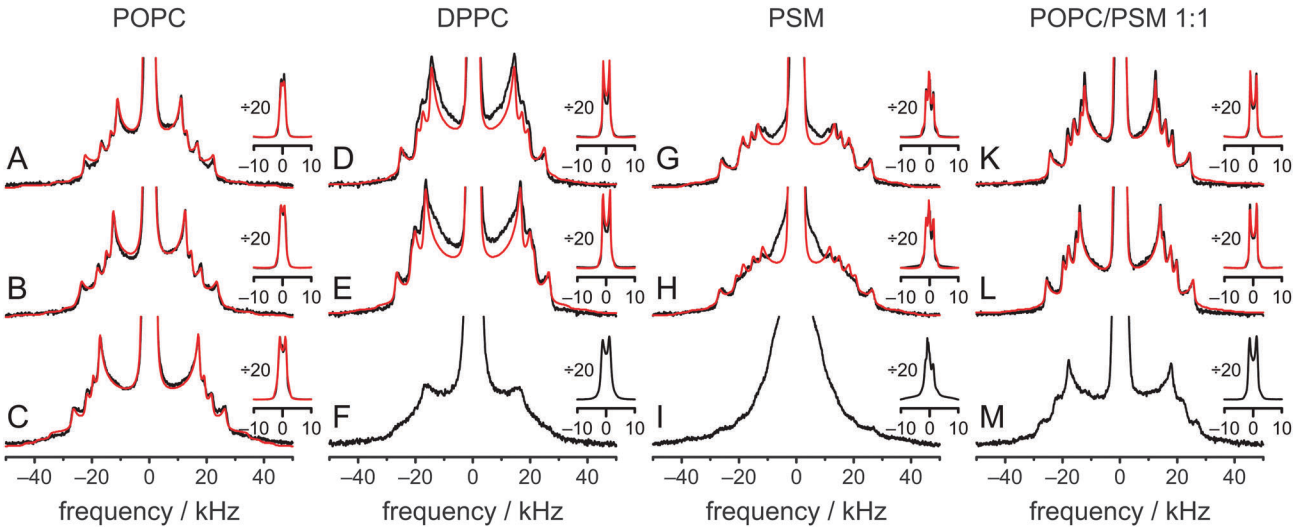


Fig. 6 $^2$H NMR spectra of cholesterol-$d_{11}$ (25 mol% relative to all other lipids) in various environments at 50 °C (A, D, G and K), 37 °C (B, E, H and L), and 5 °C (C, F, I and M). NMR spectra were measured in POPC (A–C), DPPC (D–F), PSM (G–I) and POPC/PSM (1 : 1 mol/mol) (K–M). The inset shows the same spectra vertically divided by a factor of 20 to show the intense Pake doublets from the two terminal $CH_3$ groups. Measured spectra are shown in black, while numerical fits are red.

significantly improve this condensation effect.[53] In fact, many modifications lead to dramatic reductions of this effect even if the modification was very small, such as changing a single double bond within the ring structure.[54–56] Recently, however, it has been shown that rather surprisingly, approximately half of the condensation effect is caused by the aliphatic side chain of cholesterol.[15] Furthermore, the condensation effect depends on the chain length and is highest for the natural chain length of cholesterol.[15] In addition, the condensation effect is reduced in case there is no branched methyl group at the chain end.[17]

In this article, details of the structure and dynamics of the aliphatic side chain of cholesterol and the molecular origin of the observed effects were investigated in four different membrane environments using $^2$H NMR spectroscopy and MD simulations. The general features of all experimental spectra are similar, indicating that the overall behavior of the aliphatic side chain of cholesterol is comparable in all environments. At 37 °C, the average order parameter is lowest for POPC (0.128) and highest for DPPC (0.160). Average order parameters in PSM and POPC/PSM are relatively similar (0.149 and 0.147, respectively). The lineshapes of the respective $^2$H NMR spectra, however, are rather different. In POPC and POPC/PSM, the NMR spectra are rather similar and indicate axially symmetric motions of cholesterol, while in DPPC and PSM some line broadening, possibly indicative of asymmetric behavior even at 50 °C is observed, which probably originates from incomplete rotational averaging on the NMR timescale of several microseconds. This indicates that the presence of POPC accelerates cholesterol rotational motion in PSM. At 5 °C, individual Pake doublets cannot be discriminated anymore in DPPC and PSM (see Fig. 6), while the $^2$H NMR spectra in POPC and POPC/PSM still resolve more details.

To analyze the NMR spectra in more detail, several MD simulations were conducted and overall, their agreement with experiment was very reasonable. It was exceptionally good with less than 5% deviation for the two POPC MD simulations at different temperatures, while previous MD simulations of a very similar system differed by a factor of ~2.[28] The large difference in the aliphatic side chain region of the previous MD simulation (despite of the otherwise good agreement) can be explained by the observed steric clashes as described in this article. The previous simulations used a force field with united atoms in the aliphatic side chain, which therefore could not capture the steric clashes of the involved hydrogens. Unfortunately, the steric clashes are separated by two dihedral angles (refer Fig. 4A and B). If they were separated by just one dihedral angle, the steric clashes could be incorporated into the dihedral angle force field parameters. Therefore, cholesterol force fields with united atoms in the aliphatic side chains should be used with caution.

In our study, agreement with experimental data was still reasonable for the MD simulations of cholesterol in DPPC and PSM with 16.3% and 8.7% deviation, respectively. Nevertheless, this was significantly worse than in the simulations of the POPC/cholesterol mixture. Since the agreement was good in POPC, force field inaccuracies are unlikely. However, the NMR spectra of these samples already show signs of slight axially asymmetric motion on a timescale of several microseconds (Fig. 6). Therefore, the origin of this discrepancy most likely is incomplete sampling despite the very long 1.5 μs MD simulation time. Possibly, rapid MD sampling techniques[57–59] would yield better agreement. This interpretation is supported by the relatively good agreement between experiment and simulation for the more mobile $CH_3$ groups, where sampling issues are diminished.

Therefore, the MD simulation of cholesterol in POPC at 37 °C, where agreement was excellent, was analyzed in detail. The most interesting observation in this study was that the hydrogens at C22, C23, and C24 are not magnetically equivalent and that this is caused by steric clashes of atoms within the cholesterol molecule. These clashes prevent the occurrence of certain conformations. This reduced conformational flexibility

 

is also reflected in the order parameters that were calculated for the C–D bonds in the aliphatic cholesterol side chain. These order parameters are relatively high compared to those in the methylene and methyl segments in the lipids, which are similarly deeply embedded in the bilayer[11] and comparable to those in the rigid ring determined previously.[25] It is surprising that experimental investigations showed the hydrogens on C22 to be equivalent, while those on C24 were not equivalent.[25] The steric clashes we found should lead to inequalities at both positions and our MD results are not consistent with this experimental observation, which we cannot explain at the moment.

## Conclusions

The observed steric clashes shed light on the question why the aliphatic side chain of cholesterol contributes significantly to the condensation effect of the molecule in membranes. It is located close to the methylene and methyl segments in the lipids, which exhibit the lowest order and, therefore, can be ordered to the highest extent. There, it occupies conformational space and thereby limits the conformational flexibility of the lipid acyl chains. The relatively high order that is observed for the aliphatic cholesterol side chain magnifies this effect. The prohibited conformations reduce the volume accessible to the aliphatic side chain, which reduces the number of possible conformations. In turn, this also reduces the possible conformations that the surrounding lipid acyl chains can adapt.

Interestingly, the prohibited conformations are those, in which the aliphatic side chain would stay in the plane of the cholesterol ring structure (see Fig. 4A and B). Therefore, we analyzed the positions of the C25 group when looking along the main rotational axis of cholesterol, as shown in Fig. 7. It is immediately obvious that the aliphatic side chain has a much higher tendency to move perpendicular to the ring system instead of staying within the plane of the rings. For a more detailed analysis, the chain axis was defined as the vector from C17 to C25 and the order parameter matrix for this axis calculated in the internal frame of cholesterol *via*

$$Q_{\alpha\beta} = \frac{1}{N}\sum_i \left( u_\alpha^{(i)} u_\beta^{(i)} - \frac{1}{3}\delta_{\alpha\beta} \right),$$

where $u_{\alpha/\beta}$ designates a component of the vector with the indices $\alpha, \beta = (x, y, z)$ and the sum is calculated over all $N$ molecules. This matrix was diagonalized and the order parameter $S$ and the biaxiality $B$ extracted from the diagonal elements *via*

$$Q^{\text{diagonal}} = \begin{pmatrix} \frac{2}{3}S & 0 & 0 \\ 0 & -\frac{1}{3}S + B & 0 \\ 0 & 0 & -\frac{1}{3}S - B \end{pmatrix}.$$

The resulting order parameter $S$ was 0.78 with a biaxiality $B$ of 0.046 (for the MD simulation of cholesterol in POPC at 50 °C those values were 0.76 and 0.051, respectively). These values of biaxiality are comparable to values observed for nematic liquid crystals with biaxial behavior.[60] Therefore, the forbidden conformations not only increase the order of the aliphatic side chain, but also lead to a very anisotropic mobility pattern. This possibly modulates cholesterol lipid interactions, but the implications of this behavior are not understood yet and should be investigated in the future.

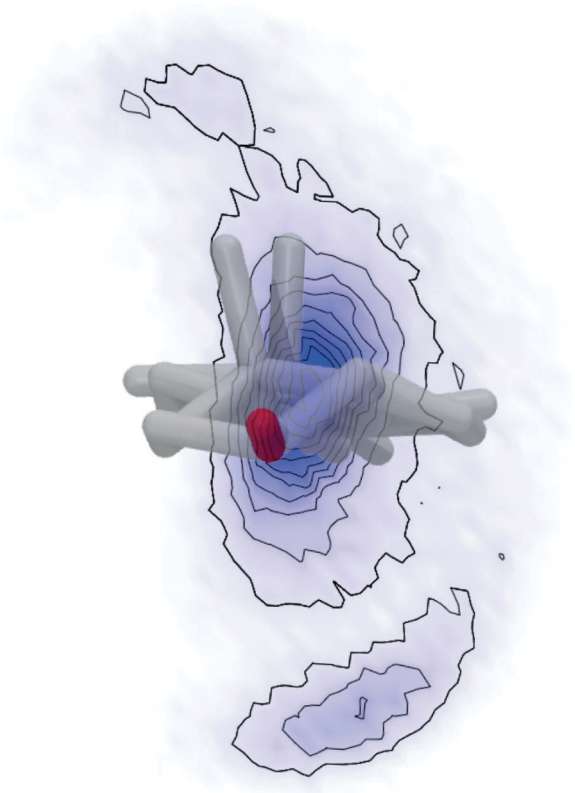

Fig. 7 Distribution of the C25 position when looking at cholesterol from the top (looking at the OH group (red) towards the aliphatic side chain along the main rotational axis of cholesterol). Hydrogens were omitted from the cholesterol structure for clarity and the two $CH_3$ groups that stick out of the plane of the cholesterol rings can be seen pointing upwards. The probability distribution of the C25 position is indicated by blue color, where more intense color corresponds to higher probability.

## Acknowledgements

The authors would like to thank Prof. Dr Norbert Sträter for useful comments on cholesterol structures. The study was supported by the Deutsche Forschungsgemeinschaft (SFB 1052, B6).

## References

1 M. G. van, D. R. Voelker and G. W. Feigenson, *Nat. Rev. Mol. Cell Biol.*, 2008, **9**, 112.
2 K. Jacobson, O. G. Mouritsen and R. G. W. Anderson, *Nat. Cell Biol.*, 2007, **9**, 7.
3 M. L. Frazier, J. R. Wright, A. Pokorny and P. F. Almeida, *Biophys. J.*, 2007, **92**, 2422.

4 A. Tsamaloukas, H. Szadkowska and H. Heerklotz, *J. Phys.: Condens. Matter*, 2006, **18**, S1125.
5 K. Simons and E. Ikonen, *Science*, 2000, **290**, 1721.
6 D. A. Brown and E. London, *Annu. Rev. Cell Dev. Biol.*, 1998, **14**, 111.
7 S. Munro, *Cell*, 2003, **115**, 377.
8 N. Shimokawa, M. Nagata and M. Takagi, *Phys. Chem. Chem. Phys.*, 2015, **17**, 20882.
9 P. F. Almeida, A. Pokorny and A. Hinderliter, *Biochim. Biophys. Acta*, 2005, **1720**, 1.
10 D. Huster, K. Arnold and K. Gawrisch, *Biochemistry*, 1998, **37**, 17299.
11 A. Bunge, P. Müller, M. Stöckl, A. Herrmann and D. Huster, *Biophys. J.*, 2008, **94**, 2680.
12 M. A. Davies, H. F. Schuster, J. W. Brauner and R. Mendelsohn, *Biochemistry*, 1990, **29**, 4368.
13 G. Orädd, V. Shahedi and G. Lindblom, *Biochim. Biophys. Acta*, 2009, **1788**, 1762.
14 E. Oldfield, M. Meadows, D. Rice and R. Jacobs, *Biochemistry*, 1978, **17**, 2727.
15 H. A. Scheidt, T. Meyer, J. Nikolaus, D. J. Baek, I. Haralampiev, L. Thomas, R. Bittman, A. Herrmann, P. Müller and D. Huster, *Angew. Chem., Int. Ed.*, 2013, **52**, 12848.
16 J. R. Robalo, J. P. Prates Ramalho, D. Huster and L. M. Loura, *Phys. Chem. Chem. Phys.*, 2015, **17**, 22736.
17 T. Meyer, D. J. Baek, R. Bittman, I. Haralampiev, P. Müller, A. Herrmann, D. Huster and H. A. Scheidt, *Chem. Phys. Lipids*, 2014, **184**, 1.
18 D. Huster, *Biochim. Biophys. Acta*, 2014, **1841**, 1146.
19 M. F. Brown, *Biochemistry*, 2012, **51**, 9782.
20 A. Leftin and M. F. Brown, *Biochim. Biophys. Acta*, 2011, **1808**, 818.
21 T. Bartels, R. S. Lankalapalli, R. Bittman, K. Beyer and M. F. Brown, *J. Am. Chem. Soc.*, 2008, **130**, 14521.
22 S. L. Veatch, O. Soubias, S. L. Keller and K. Gawrisch, *Proc. Natl. Acad. Sci. U. S. A.*, 2007, **104**, 17650.
23 A. Leftin, T. R. Molugu, C. Job, K. Beyer and M. F. Brown, *Biophys. J.*, 2014, **107**, 2274.
24 M. G. Taylor, T. Akiyama, H. Saito and I. C. Smith, *Chem. Phys. Lipids*, 1982, **31**, 359.
25 E. J. Dufourc, E. J. Parish, S. Chitrakorn and C. P. Smith, *Biochemistry*, 1984, **23**, 6062.
26 P. Schmidt, L. Thomas, P. Müller, H. A. Scheidt and D. Huster, *Chemistry*, 2014, **20**, 4986.
27 L. Thomas, J. Kahr, P. Schmidt, U. Krug, H. A. Scheidt and D. Huster, *J. Biomol. NMR*, 2015, **61**, 347.
28 T. M. Ferreira, F. Coreta-Gomes, O. H. Ollila, M. J. Moreno, W. L. Vaz and D. Topgaard, *Phys. Chem. Chem. Phys.*, 2013, **15**, 1976.
29 K. Gawrisch, N. V. Eldho and I. V. Polozov, *Chem. Phys. Lipids*, 2002, **116**, 135.
30 K. Mors, C. Roos, F. Scholz, J. Wachtveitl, V. Dotsch, F. Bernhard and C. Glaubitz, *Biochim. Biophys. Acta*, 2013, **1828**, 1222.
31 M. Holtje, T. Forster, B. Brandt, T. Engels, R. W. von and H. D. Holtje, *Biochim. Biophys. Acta*, 2001, **1511**, 156.
32 D. J. Baek and R. Bittman, *Chem. Phys. Lipids*, 2013, **175–176**, 99.
33 J. H. Davis, K. R. Jeffrey, M. Bloom, M. I. Valic and T. P. Higgs, *Chem. Phys. Lett.*, 1976, **42**, 390.
34 S. Jo, T. Kim and W. Im, *PLoS One*, 2007, **2**, e880.
35 J. C. Phillips, R. Braun, W. Wang, J. Gumbart, E. Tajkhorshid, E. Villa, C. Chipot, R. D. Skeel, L. Kale and K. Schulten, *J. Comput. Chem.*, 2005, **26**, 1781.
36 J. B. Klauda, R. M. Venable, J. A. Freites, J. W. O'Connor, D. J. Tobias, C. Mondragon-Ramirez, I. Vorobyov, A. D. MacKerell Jr and R. W. Pastor, *J. Phys. Chem. B*, 2010, **114**, 7830.
37 J. B. Lim, B. Rogaski and J. B. Klauda, *J. Phys. Chem. B*, 2012, **116**, 203.
38 R. M. Venable, A. J. Sodt, B. Rogaski, H. Rui, E. Hatcher, A. D. MacKerell, Jr., R. W. Pastor and J. B. Klauda, *Biophys. J.*, 2014, **107**, 134.
39 U. Essmann, L. Perera, M. L. Berkowitz, T. Darden, H. Lee and L. G. Pedersen, *J. Chem. Phys.*, 1995, **103**, 8577.
40 W. van Gunsteren and H. J. C. Berendsen, *Mol. Phys.*, 1977, **34**, 1311.
41 J. H. Davis, *Biochim. Biophys. Acta*, 1983, **737**, 117.
42 J. Seelig, *Q. Rev. Biophys.*, 1977, **10**, 353.
43 H. I. Petrache, S. W. Dodd and M. F. Brown, *Biophys. J.*, 2000, **79**, 3172.
44 M. F. Brown, S. Lope-Piedrafita, G. V. Martinez, H. I. Petrache, in *Modern Magnetic Resonance*, ed. G. Webb, Springer, Heidelberg, 2006, pp. 241–252.
45 A. Vogel, H. A. Scheidt, S. E. Feller, J. Metso, R. M. Badeau, M. J. Tikkanen, K. Wahala, M. Jauhiainen and D. Huster, *Biophys. J.*, 2014, **107**, 114.
46 H. S. Shieh and C. E. Nordmann, *Acta Crystallogr., Sect. E: Crystallogr. Commun.*, 2002, **58**, 079.
47 R. J. Galloway, S. A. Raza, R. D. Young and I. D. H. Oswald, *Cryst. Growth Des.*, 2012, **12**, 231.
48 H. S. Shieh, L. G. Hoard and C. E. Nordmann, *Acta Crystallogr., Sect. B: Struct. Crystallogr. Cryst. Chem.*, 1981, **37**, 1538.
49 L. Y. Hsu, J. W. Kampf and C. E. Nordman, *Acta Crystallogr., Sect. B: Struct. Sci.*, 2002, **58**, 260.
50 R. S. Rowland and R. Taylor, *J. Phys. Chem.*, 1996, **100**, 7384.
51 W. G. Wu and L. M. Chi, *J. Am. Chem. Soc.*, 1991, **113**, 4683.
52 O. G. Mouritsen and M. J. Zuckermann, *Lipids*, 2004, **39**, 1101.
53 T. Rog, M. Pasenkiewicz-Gierula, I. Vattulainen and M. Karttunen, *Biophys. J.*, 2007, **92**, 3346.
54 H. A. Scheidt, P. Müller, A. Herrmann and D. Huster, *J. Biol. Chem.*, 2003, **278**, 45563.
55 D. Huster, H. A. Scheidt, K. Arnold, A. Herrmann and P. Müller, *Biophys. J.*, 2005, **88**, 1838.
56 S. Milles, T. Meyer, H. A. Scheidt, R. Schwarzer, L. Thomas, M. Marek, L. Szente, R. Bittman, A. Herrmann, P. T. Gunther, D. Huster and P. Müller, *Biochim. Biophys. Acta*, 2013, **1828**, 1822.
57 A. Vogel, G. Reuther, M. B. Roark, K. T. Tan, H. Waldmann, S. E. Feller and D. Huster, *Biochim. Biophys. Acta*, 2010, **1798**, 275.
58 Y. M. Rhee and V. S. Pande, *Biophys. J.*, 2003, **84**, 775.
59 D. Hamelberg, J. Mongan and J. A. McCammon, *J. Chem. Phys.*, 2004, **120**, 11919.
60 K. Severing and K. Saalwächter, in *Thermotropic Liquid Crystals*, ed.A. Ramamoorthy, Springer, Berlin, 2007, ch. 5, pp. 141–170.